SEGMENTATION AND DETECTION OF NUCLEI IN SILVER STAINED CELL SPECIMENS FOR EARLY CANCER DIAGNOSIS

André A. Bell[1]*, Gerlind Herberich*[1]*, Dietrich Meyer-Ebrecht*[1]*, Alfred Böcking*[2]*, Til Aach*[1]

Email: andre.bell@lfb.rwth-aachen.de
[1]Institute of Imaging and Computer Vision, RWTH Aachen University, 52056 Aachen, Germany
[2]Institute for Cytopathology, Heinrich-Heine-University Düsseldorf, 40225 Düsseldorf, Germany

ABSTRACT

For successful cure, cancer has to be detected as early as possible. Since cancer starts from a single cell, this can best be done using cytopathological methods. One important diagnostically relevant measure is the proliferation rate of the cells, which can be estimated from segmented silver stained nuclei. However, the microscopy images of silver stained specimens vary strongly in intensity and contrast and are furthermore compromised by an overall texture.

We show that a precise segmentation of the nuclei is possible using a two-step approach. First, an oversegmentation with the mean shift algorithm is obtained. In a second step, these regions are merged to objects, guided by a suitable shape model, viz an ellipse, but simultaneously allowing deviations from this shape model. The segmentation results are compared to a gold standard of 8617 nuclei from 23 specimens of the thyroid gland, achieving a mean areal segmentation error of $\Delta\bar{A}_{\text{nucleus}} = 12\mu m^2$ per nucleus.

Index Terms— silver stain, microscopy images, nuclear segmentation, mean shift algorithm, region grouping

1. INTRODUCTION

Cancer is one of the foremost reasons of death in industrial countries. To counteract the consequences of cancer, the disease has to be detected and treated early. This can best be achieved at *cellular* level, to detect the earliest onset of a tumor. The cell specimens can be analyzed microscopically with a variety of diagnostic methods. Besides routinely used methods, the proliferation of suspicious cells is diagnostically relevant, since high proliferation indicates cancer.

One method to measure the proliferation rate of cells is to analyze the cells after silver staining. Silver is accumulated on active nucleolar organizer regions (AgNORs) within the nuclei. These AgNORs can be observed with a microscope as dark, spot-like regions (Fig. 1). Their count and area within each nucleus may be taken as a measure of the amount of protein synthesis, which is related to the proliferation rate. It has been shown that this is a diagnostically highly relevant criterion for different types of cancer [1, 2, 3]. For cytological diagnosis of cancer of, e.g., the oral mucosa [2], the sensitivity has thus been increased from 97% to 100%. Furthermore, the AgNOR area, measured on fine needle aspiration biopsies from the thyroid gland, allowed to *preoperatively* distinguish between adenoma and carcinoma [4].

In previous work we have developed methods to automatically analyze AgNORs [5, 6]. This analysis in turn requires that the nuclei have to be segmented and detected within the microscopy images first.

2. STATE OF THE ART

To segment nuclei in images of commonly used cell stainings, e.g., Papanicolaou or May-Grünwald-Giemsa, methods based on level-sets [7], region-growing [8], mean shift segmentation [9] and active contours [10, 11] have been developed. Unlike these stainings, however, images of silver stained specimens are afflicted by strong *variations* of both contrast and intensity (Fig. 1).

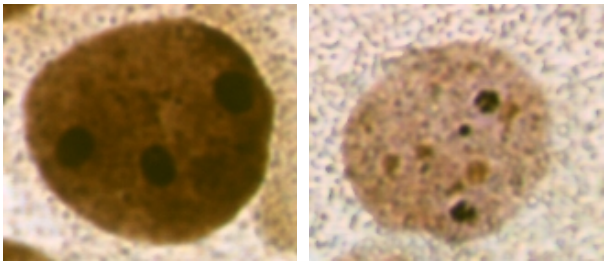

Fig. 1. Two silver stained nuclei from epithelial cells of the thyroid. Note the artifacts ("snow") and variations in contrast and intensity. These variations are observable even within one specimen. Inside the nuclei, the AgNORs (dark, spot-like regions) can be seen.

These variations appear on different specimens as well as within one specimen. Furthermore, the images may be compromised by an overall texture. Hence, a-priori knowledge, i.e., a geometric model, has to be incorporated into the seg-

The project is supported by the Viktor and Mirka Pollak Fund for Biomedical Engineering.

mentation algorithm. Deviations from this model have to be allowed since nuclei may vary in shape and size. The proposed segmentation of silver stained nuclei thus consists of two steps: an oversegmentation with the mean shift algorithm followed by a shape model-guided region merging.

3. MEAN SHIFT SEGMENTATION

To segment nuclei and subcellular features like AgNORs, the segmentation algorithm must consider color-similarity as well as local connectivity. It has been shown that good results for image segmentation [12] can be achieved with the mean shift algorithm [9, 13, 14]. The mean shift algorithm is an unsupervised clustering algorithm based on a kernel density estimate [9]

$$\hat{f}(\mathbf{x}) = \frac{1}{nh^d} \sum_{i=1}^{n} K(\frac{\mathbf{x} - \mathbf{x}_i}{h}) \tag{1}$$

where $\mathbf{x}_i \in \mathbb{R}^d$, $i = 1..n$, are n feature vectors and h is the window radius of the used kernel K. Let the mean shift vector $\mathbf{m}(\mathbf{x})$ be defined as a vector proportional to the normalized density gradient estimate

$$\mathbf{m}(\mathbf{x}) \propto \frac{\hat{\nabla} f_{K_1}}{\hat{f}_{K_2}}. \tag{2}$$

Thus, the mean shift vector is always directed towards the maximum increase in the density function. Choosing K_1 to be the Epanechnikov kernel and K_2 to be the Flat kernel, it can be shown that

$$\mathbf{m}(\mathbf{x}) = \frac{1}{N_x} \sum_{\mathbf{x}_i \in S_h(\mathbf{x})} (\mathbf{x}_i - \mathbf{x}) \tag{3}$$

where $S_h(\mathbf{x})$ is the d-dimensional unit sphere [9, 13]. Iterative calculation of the mean shift vector and shifting the kernel window by this vector will converge close to a point with zero gradient [9], i.e., to a mode. This efficiently seeks, for every feature vector $\mathbf{x}_i$, the corresponding mode on the underlying density function.

For image segmentation, every pixel is assigned a feature vector, which is composed of the spatial location of the pixel and its color value in the $L^*u^*v^*$-color space. To account for different scaling of the spatial space and the color space, we use an anisotropic kernel window (h_s, h_c) [9]. The clusters found by the mean shift algorithm form the image segments containing adjacent pixels with a certain similarity in color.

Modes closer than h_s and h_c are grouped into one segment. Subsequently, spurious segments with fewer pixels than some threshold may be merged to similar modes [9].

The mean shift algorithm allows to calculate a specific amount of oversegmentation such that the segment boundaries include all edges, which are part of the sought nucleus contour. Due to the precision of these boundaries it is not necessary to improve their position. Hence, adjacent segments belonging to one object can now be grouped together [15].

4. REGION GROUPING

An intuitive model for a nucleus is an ellipse, which is described through its centroid $(\bar{x}, \bar{y})$, its orientation ϕ and the lengths of the two principal axes (the shape parameters) $\mathbf{a}$. Hence, the parameter vector $\mathbf{a}$ allows an anisotropic scaling of the ellipse. Let g_i be a set of adjacent segments, which is to be checked for merging. Based on the central moments

$$\mu_{pq} = \sum_{x,y \in g_i} (x - \bar{x})^p (y - \bar{y})^q \tag{4}$$

of the group g_i, the covariance matrix $\mathbf{C}$

$$\mathbf{C} = \frac{1}{\mu_{00}} \begin{pmatrix} \mu_{20} & \mu_{11} \\ \mu_{11} & \mu_{02} \end{pmatrix} \tag{5}$$

and the corresponding larger eigenvalue λ_1 and eigenvector $\mathbf{v}_1$, with $\mathbf{C} \cdot \mathbf{v}_1 = \lambda_1 \cdot \mathbf{v}_1$, can be calculated. This then allows to estimate the orientation of an elliptic approximation for g_i by

$$\phi = \arctan \left(\frac{\lambda_1 - \mu_{20}/\mu_{00}}{\mu_{11}/\mu_{00}} \right) \tag{6}$$

After rotating the group g_i by $-\phi$ around the centroid, the parameter vector $\mathbf{a}$ can be estimated from the distance between centroid and horizontal and vertical extent of the group g_i. This first estimate can then be refined in order to achieve best possible area overlapping of g_i and its elliptic approximation. We used the downhill-simplex-algorithm [16] for optimization.

We assume that the parameter vector $\mathbf{a}$ follows a Gaussian distribution for the nuclei. Hence, we have calculated the mean parameter vector $\bar{\mathbf{a}}$ and the corresponding covariance matrix $\mathbf{\Sigma}$ on a representative set of $N = 85$ independent, segmented, and reviewed nuclei. Consequently, the probability of the group g_i to be a nucleus is given by

$$p(\mathbf{a}) = \frac{1}{(2\pi)^{N/2} |\mathbf{\Sigma}|^{1/2}} e^{-\frac{1}{2} \tilde{\mathbf{a}}^T \mathbf{\Sigma}^{-1} \tilde{\mathbf{a}}}, \ \tilde{\mathbf{a}} = \mathbf{a} - \bar{\mathbf{a}}. \tag{7}$$

A group g_i can differ considerably from the elliptic shape. We take this into account by a cost function $E(g_i)$ which assesses how likely it is that the group g_i is a nucleus. $E(g_i)$ is composed of two components weighted by β:

$$E(g_i) = (1 - \beta) E_{\text{DeformShape}} + \beta E_{\text{DeformSize}} \tag{8}$$

with

$$E_{\text{DeformShape}} = \frac{A_{g_i} A_{\text{ellipse}}}{A_C^2} \frac{1}{\kappa} \ ; \ \kappa = \frac{A_{g_i}}{c_{g_i}^2} \tag{9}$$

and

$$E_{\text{DeformSize}} = \tilde{\mathbf{a}}^T \mathbf{\Sigma}^{-1} \tilde{\mathbf{a}} \ ; \ \tilde{\mathbf{a}} = \mathbf{a} - \bar{\mathbf{a}} \tag{10}$$

where A_{g_i}, A_{ellipse} and A_C are the area of the group, the area of the ellipse, and the common area, respectively; κ the compactness and c_{g_i} the circumference of the group g_i. To assess

the improvement contributed by a newly formed grouping to the partition of the entire image, $E(g_i)$ is incorporated into a global cost

$$E_{\text{global}} = (1-\gamma)\Big[\sum_{i=1}^{n} \xi_i E(g_i)\Big] + \gamma n \; ; \; \xi_i = \frac{A_{g_i}}{\sum_j A_{g_j}} \quad (11)$$

with n being the number of groupings within the partition, and γ a weighting factor. Consistent with the *minimum-description-length*-principle [15], this approach prefers a simple partition of the image over a partition into many small regions.

Since a full search over all possible groups of segments is not feasible, the groups have to be selected appropriately. Therefore, we set up a region adjacency graph for all segments in the image. Based on the Euclidian distance of the mean color value and variance between neighboring segments, we start by selecting the closest segments first. For the largest region in such a set of adjacent regions, we consider its combination with each of its neighboring regions as group g_i and compute the global cost that would result from merging this group. The first of the tested combinations, that leads to an improvement of the global cost, is merged. This is repeated until no further decrease of the global cost is possible.

5. EXPERIMENTS, RESULTS AND DISCUSSION

We acquired 4006 images of 23 specimens of the thyroid gland in two stains (Table 1). Rather than directly applying the silver stain, these specimens were first stained using the so-called Feulgen stain, where the nuclei in general appear very clearly. An accurate segmentation of the nuclei in this staining is obtained as decribed in [17]. After review by an experienced cytopathologist, these segmentations provide the gold standard against which the segmentation results for silver stain obtained by the described algorithm are compared. Note that, in contrast to a gold standard created by pure manual segmentation by an expert, this procedure reduces the influences of inter- and intra-individual variability. After de-staining to remove the Feulgen stain and subsequent re-staining with silver nitrate, images of the *same* cells were acquired and registered [17] to their corresponding Feulgen images. For corresponding nuclei segmentations between the Feulgen reference and the silver stain data, we calculated the non-overlapping area (symmetric difference) per nucleus $\Delta A = A_{\text{Feulgen}} \triangle A_{\text{silver}}$. Results for individual nuclei from images of different specimens are shown in Fig. 2. Note that the fourth nucleus in Fig. 2 strongly differs from the elliptic shape model, but was still segmented correctly. The segmentation precision achieved on the silver stained specimens ranges from $\Delta A = 4.8\mu m^2$ (best) to $\Delta A = 41.96\mu m^2$ (worst). The mean segmentation precision over all 23 specimens is $\Delta \bar{A}_{\text{nucleus}} = 12\mu m^2$. Further numerical results are given in Table 1. These results have been obtained setting $\gamma = 0.002$ and $\beta = 0.008$ for all images. The kernel radius h has been chosen slide-specifically as inter-slide variations in contrast are much more significant than intra-slide variations. For 78% of the slides we set $h_s = h_c = 14$.

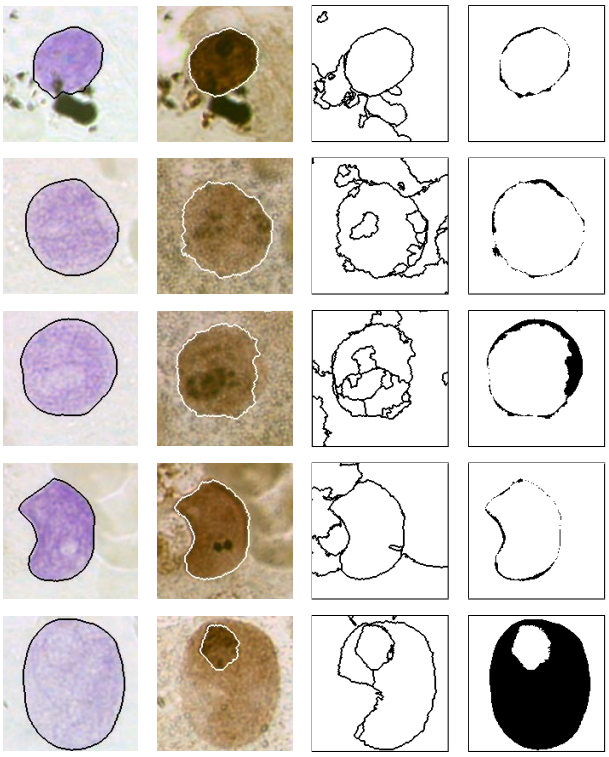

Fig. 2. Example results for nuclei segmentations. Each row shows another nucleus of a cell from the thyroid. Column (a) shows the nuclei stained according to Feulgen with corresponding gold standard segmentations. In column (b) the corresponding images of the identical nuclei in the silver stain are shown with their segmentation results. The intermediate mean shift oversegmentation result and the segmentation error with respect to the goldstandard are shown in column (c) and (d) respectively. The nucleus in the first row is from a specimen (No. 19 in table 1) with a strong contrast between nucleus and cytoplasm. Note the precise segmentation despite the presence of dirt particles. In rows 2 and 3 examples of nuclei of a specimen (No. 23 in table 1) with low contrast and strong staining artifacts are shown. Row 4 (No. 12 in table 1) gives an example of a nucleus with strong deviation from the geometric model. Finally, row 5 contains a nucleus from a specimen (No. 6 in table 1) with strong intra–nuclear staining variability such that large AgNOR–clusters are detected as objects, which significantly increases the mean segmentation error $\Delta \bar{A}_{\text{nucleus}}$.

We have shown that reliable segmentations of nuclei in silver stained cell specimens is feasible, even though the staining quality may vary strongly from nucleus to nucleus even on the same slide. Our segmentation algorithm is based on an intermediate oversegmentation acquired with the mean shift al-

specimen	No. images	No. cells	$\Delta\bar{A}_{\text{nucleus}}$
1	144	356	7.51
2	196	450	9.65
3	90	315	11.09
4	156	274	8.23
5	173	173	26.45
6	245	377	41.96
7	168	405	7.22
8	157	668	9.86
9	244	300	14.24
10	106	196	21.20
11	190	337	28.06
12	187	301	11.90
13	242	491	7.63
14	207	421	6.47
15	226	176	14.00
16	186	508	7.98
17	134	581	9.35
18	140	330	6.31
19	140	640	4.80
20	165	573	10.69
21	174	135	9.19
22	147	332	11.42
23	189	278	16.20
all	4006	8617	12.00

Table 1. Results of our experiments. For each specimen this table shows the number of images (No. images), the number of detected cells within these images (No. cells) and the mean difference between the segmented nuclear area compared to the gold standard in μm^2 ($\Delta\bar{A}_{\text{nucleus}}$).

gorithm. The regions of the oversegmentation are then merged, guided by a shape model for the nuclei, which leads to a successful segmentation for almost every isolated nucleus. Due to the shape model, the segmentation fails for nuclei touching each other, overlapping nuclei, and lytic nuclei. Since the latter two cases are irrelevant for diagnosis, our segmentation provides the basis for a fully automatic analysis of cell nuclei in silver stained specimens. To also include pairs of nuclei touching one another, extending the shape model to also represent these, is already underway.

6. REFERENCES

[1] L. Shechtman, R. Koren, A. Horowitz, I. Shechtman, M. Halpern, and R. Gal, "Diagnostic value of AgNOR staining in thyroid cytology," *Anal Quant Cytol Histol*, vol. 20, no. 3, pp. 187–91, 1998.

[2] T. W. Remmerbach, H. Weidenbach, C. Muller, A. Hemprich, N. Pomjanski, B. Buckstegge, and A. Böcking, "Diagnostic value of nucleolar organizer regions (AgNORs) in brush biopsies of suspicious lesions of the oral cavity," *Anal Cell Pathol*, vol. 25, no. 3, pp. 139–146, 2003.

[3] J. S. Misra, V. Das, A. N. Srivastava, U. Singh, and M. Singh, "AgNOR counts in cervical smears under normal and other cytopathologic conditions," *Anal Quant Cytol Histol*, vol. 27, no. 6, pp. 337–340, 2005.

[4] D. Slowinska-Klencka, M. Klencki, B. Popowicz, and A. Lewinski, "AgNOR quantification in the diagnosis of follicular pattern thyroid lesions," *Anal Quant Cytol Histol*, vol. 25, no. 6, pp. 347–352, 2004.

[5] A. A. Bell, J. N. Kaftan, T. Aach, D. Meyer-Ebrecht, and A. Böcking, "High Dynamic Range Images As a Basis for Detection of Argyrophilic Nucleolar Organizer Regions Under Varying Stain Intensities," in *IEEE International Conference on Image Processing, ICIP 2006*. 2006, pp. 2541–2544, IEEE.

[6] J. N. Kaftan, A. A. Bell, D. Meyer-Ebrecht, A. Böcking, and T. Aach, "Segmentation of Nucleolar Organizer Regions by Means of High Dynamic Range Cell Imaging and Analysis," in *11th Workshop Vision, Modeling, and Visualization 2006*, 2006, pp. 285–292.

[7] J. A. Sethian, *Level set methods and fast marching methods*, Cambridge University Press, 2 edition, 2002.

[8] U. Adiga, R. Malladi, R. Fernandez-Gonzalez, and C. Ortiz, "High-Throughput Analysis of Multispectral Images of Breast Cancer Tissue," *IEEE Transactions on Image Processing*, vol. 8, pp. 2259–2268, 2006.

[9] D. Comaniciu and P. Meer, "Mean Shift: A Robust Approach Toward Feature Space Analysis," *IEEE Transactions on Pattern Analysis and Machine Intelligence*, vol. 24, no. 5, pp. 603–619, 2002.

[10] T. McInerney and D. Terzopoulos, "Deformable models in medical image analysis: A survey," *Medical Image Analysis*, vol. 1, no. 2, pp. 91–108, 1996.

[11] N. Ray, S. T. Acton, and K. Ley, "Tracking leukocytes in vivo with shape and size constrained active contours," *IEEE Transactions on Medical Imaging*, vol. 21, no. 10, pp. 1222–1235, 2002.

[12] J. S. Suri, S. K. Setarehdan, and S. Singh (Eds), *Advanced Algorithmic Approaches to Medical Image Segmentation*, Springer, 2002.

[13] K. Fukunaga and L. D. Hostetler, "The Estimation of the Gradient of a Density Function, with Applications in Pattern Recognition," *IEEE Transactions on Information Theory*, vol. 21, no. 1, pp. 32–40, 1975.

[14] Y. Cheng, "Mean Shift, Mode Seeking, and Clustering," *IEEE Transactions on Pattern Analysis and Machine Intelligence*, vol. 17, no. 8, pp. 790–799, 1995.

[15] S. Sclaroff and L. Liu, "Deformable shape detection and description via model-based region grouping," *IEEE Transactions on Pattern Analysis and Machine Intelligence*, vol. 23, no. 5, pp. 475–489, 2001.

[16] W. H. Press, S. A. Teukolsky, W. T. Vettering, and B. P. Flannery, *Numerical Recipes in C++: The Art of Scientific Computing*, Cambridge University Press, 2002.

[17] T. Würflinger, J. Stockhausen, D. Meyer-Ebrecht, and A. Böcking, "Robust Automatic Coregistration, Segmentation, and Classification of Cell Nuclei in Multimodal Cytopathological Microscopic Images," *Computerized Medical Imaging and Graphics*, vol. 28, pp. 87–98, 2004.